9950-950

DRL No. 198
DRD Line Item No. SE-3

DOE/JPL-956525-83/4
Distribution Category UC-63

SURFACE AND ALLIED STUDIES IN SILICON SOLAR CELLS

ANNUAL ~~Final~~ Report

For Period Covering
June 24, 1983 - June 23, 1984

By:

F. A. Lindholm
UNIVERSITY OF FLORIDA
Department of Electrical Engineering
Gainesville, FL 32611

JPL Contract No. 956525

The JPL Low-Cost Silicon Solar Array Project is sponsored by the U.S. Department of Energy and forms part of the Solar Photovoltaic Conversion Program to initiate a major effort toward the development of low-cost solar arrays. This work was performed for the Jet Propulsion Laboratory, California Institute of Technology, by agreement between NASA and DOE.

This work was performed for the Jet Propulsion Laboratory, California Institute of Technology, and was sponsored by the U. S. Department of Energy through an agreement with the National Aeronautics and Space Administration.

ACKNOWLEDGMENTS

The author would like to thank the following people who helped improve the content of this report: first, Professor Arnost Neugroschel, who contributed many useful ideas and helped lead the experimental investigations; second, Professors C. T. Sah and P. T. Landsberg, who assisted via many discussions this past year and previously on fundamentals of subjects related to those reported here; third, Peter Iles, who contributed ideas and is providing technical support, for work concerning tne passivations of surfaces; fourth, Taher Daud, who went well beyond his role as technical monitor of this contract, in providing ideas and samples and critiques that enabled improved results and presentations; fifth, members of the JPL Advisory Group, including Taher Daud, Peter Iles, Professor Martin Wolf, Gene Ralph, Professor Gunter Schwuttke, and Professor Joseph Loferski, whose intelligent questioning led to my development of Appendix A; and, finally, J. J. Liou and T. W. Jung, whose diligence and abilities as graduate research students contributed decisively to the findings reported.

Carole Boone and Carolyn McGilvray typed the report and recast equation numbers, references, and the orientation of some illustrations to provide an attractive appearance and a properly sequential presentation.

Whether the presentation is consequential or not, of course, is the responsibility of the author.

TABLE OF CONTENTS

ABSTRACT

Measuring small-signal admittance versus frequency and forward bias voltage together with a new transient measurement apparently provides the most reliable and flexible method available for determining back surface recombination velocity and low-injection lifetime of the quasineutral base region of silicon solar cells. The new transient measurement reported here is called short-circuit-current decay (SCCD). In this method, forward voltage equal to about the open-circuit or the maximum power voltage establishes excess holes and electrons in the junction transition region and in the quasineutral regions. The sudden application of a short circuit causes an exiting of the excess holes and electrons in the transition region within about ten picoseconds. From observing the slope and intercept of the subsequent current decay, one can determine the base lifetime and surface recombination velocity. The admittance measurement previously mentioned then enters to increase accuracy particularly for devices for which the diffusion length exceeds the base thickness. Detailed mathematical treatment and phenomenological reasoning provides support for the measurements reported and for the view that the method described is superior to others now existing.

The measurment of surface recombination velocity is integrated with new findings about decreased values of this parameter attained via a CVD polysilicon/silicon interface.

I. INTRODUCTION

A main purpose of this study is to establish methodologies by which one can experimentally determine, with good accuracy, the recombination parameters of silicon solar cells. These parameters include carrier lifetimes in the quasinuetral base region and the back surface recombination velocity including the velocities at internal surfaces such as those formed by a BSF region. The methodologies sought would fill a gap in the existing capabilities to measure accurately such parameters, a gap whose presence is apparently not fully understood by some workers in the field. The methodologies sought are to be flexible, in the sense that they would apply to a wide range of different solar-cell designs and in the sense that a subset of them would work for in-process control in manufacturing. Further, we seek methodologies firmly rooted in physical theory to avoid thereby possible misinterpretations of data and to provide quantitative grounds for comparisons of different experimental techniques.

A review of literature will suggest the existence of some confusion concerning surface recombination velocities. Thus we offer remarks to aid understanding of the underlying physics and of the measurement of recombination parameters.

Insofar as minority carriers are concerned, in a one-dimensional model one may regard a solar cell as a p/n junction diode bounded by front and back surfaces characterized by surface recombination velocities: S_{front} and S_{back}. The surfaces may be free surfaces, constituted perhaps of a mixture of metal and thermal oxide, or internal surfaces, such as those adjoining the low-high junction that constitutes a back-surface field (BSF) region. This characterization places emphasis on the recombination that can take place at the surfaces, though it includes volume recombination within the cell.

For well over a decade, workers in photovoltaics have understood that the presence of a low-high junction in the BSF cell can yield an effective surface recombination velocity S_{back} on the low-doped side of the low-high junction that can be orders of magnitude below the surface recombination velocity at an ohmic contact (which is o the order of 10^6 cm/s). Accurate measurement of S_{back}, together with that of carrier lifetime in the quasi-enutral base, however, has presented problems.

More recently the importance of passivating the front surface recombination velocity to increase the power conversion efficiency has become recognized. The first recognition of this importance, by Iles, appeared in a final report (NASA 1974) of narrow distribution. The first full discussion of the importance of S_{front} in the journal literature, which emphasized experimental evidence in conjunction with a modeling of highly doped Si, by Fossum, Lindholm, and Shibib (1979), met with resistance at the outset because of the inertia of the dead-layer concept of Allison and Lindmayer (1973) of early solar-cell theory. Gradually an appreciation of the importance of S_{front} has emerged. One may conjecture that this emergence resulted in part from the understanding that the huge drift field acting on minority carriers in a diffused front layer that arises in customary Si p/n junction theory is absent because of the dependence of the Si energy gap on the shallow-level dopant concentration.

Thus we recover the model stated in the first sentence of this INTRODUCTION: the view that a solar cell is a p/n junction bounded by front and back surfaces characterized by S_{front} and S_{back}. We stress the importance of experimentally determining S_{front} and S_{back}, including the determination as a function of the fabrication steps used in manufacturing.

From a theoretical viewpoint, this model yields to existing approaches for the standard solar-cell conditions: steady state (time independence) of the excitation (applied voltage or illumination). But from an experimental standpoint, steady-state excitation will not suffice for a widely applicable experimental determination of S_{front}, S_{back}, and other parameters (such as carrier lifetime) needed for informed design. Moreover, the rapidity of measurement by transient response of these parameters makes transient measurements, if accurate, attractive for in-process control at key steps in manufacturing. As we shall see, the use also of the real and imaginary parts of the small-signal admittance as a function of frequency ω and forward voltage V provides a powerful adjunct to transient measurements.

A secondary purpose of this research is to advance the understanding of decreases in surface recombination velocity afforded by polysilicon/silicon heterojunctions at free surfaces.

In the presentation to follow we first outline a mathematical method that systematically and compactly describes the large-signal transient and small-signal frequency responses of solar cells and of related devices such as transistors and diodes. This mathematical framework unifies the comparison of available methods for determining carrier recombination lifetime and surface recombination velocity of quasi-neutral principal regions of the devices.

Second, exploiting this description, we survey the adequacy of various experimental large-signal transient methods for deducing these parameters. The survey is indicative, not exhaustive.

Third, we examine in detail, both theoretically and experimentally a method that apparently has not been much explored previously. We demonstrate that this method yields both the back surface recombination velocity and the recombination lifetime of the quasi-neutral base from a single transient

measurement. To increase sensitivity and widen the range of different solar cells for which accurate experimental determinations can be made, we describe various methods that involve measuring admittance as a function of frequency and forward voltage.

Finally we briefly describe experimental research indicating the efficacy of the polysilicon/silicon heterojunction for decreasing surface recombination velocity.

2. MATHEMATICAL FRAMEWORK FOR UNIFYING VIEW OF TRANSIENT RESPONSES AND SMALL-SIGNAL RESPONSES

Here we develop a mathematical framework which could be applicable to most of the large-signal transient measurement methods and could include small-signal admittance methods for the determination of the lifetime and the back surface recombination velocity of the base region of a diode or a solar cell. This analysis will treat the minority-carrier density and the minority-carrier current in a quasi-neutral base region in low injection. Focusing on the quasi-neutral base, assumed to be n-type here (of x-independent donor density N_{DD}) with no loss in generality, will simplify the treatment. Extensions to the quasi-neutral emitter are straightforward, provided one inserts the physics relevant to n+ or p+ regions.

Assume a p^+/n diode in which the uniformly doped quasi-neutral base starts at $x = 0$ and has a general contact defined by arbitrary effective surface recombination velocity S_{eff} at the far edge $x = X_{QNB}$. Such a contact could result, for example, from a back-surface-field (BSF) region. Assume also low-level injection and uniform doping of the base region. Then a linear continuity (partial differential) equation describes the excess minority holes $p(x,t)$:

$$\partial p(x,t)/\partial t = D_p \partial^2 p(x,t)/\partial x^2 - p(x,t)/\tau_p \quad , \tag{1}$$

where D_p is the diffusion coefficient and τ_p is the lifetime of holes.

If we take the Laplace transform of (1) with respect to time, we get an ordinary differential equation in x with parameter s:

$$-p(x,0^-) + sP(x,s) = D_p \, d^2P(x,s)/dx^2 - P(x,s)/\tau_p \quad , \tag{2}$$

where

$$P(x,s) = \int_{t=0}^{t=\infty} e^{-st} p(x,t)dt \quad , \quad s = \sigma + j\omega, \; j = (-1)^{1/2} \tag{3}$$

and where $p(x,0^-)$ is the initial condition for the excess hole density. Here, $t = 0^-$ denotes infitesimal negative time, and we shall treat transient excitation for which $p(x,t)$ is in the steady state for $t < 0$.

Thus $P(x) = p(x,t)$, $t<0$ where here capital P denotes a steady-state excess hole density.

Solving Eq. (2) yields

$$P(x,s) = p(x,0^-)/s + M_1 \exp(-x/L_p^*) + M_2 \exp(x/L_p^*) \tag{4}$$

where $L_p^* = (D_p\tau_p)/(1 + s\tau_p)^{1/2}$ and where M_1 and M_2, given below, are to be determined by the boundary values at the two edges of the quasi-neutral base region: $P(0,s)$ at $x=0$, and $P(X_{QNB},s)$ at $x=X_{QNB}$. Substitution of (4) into (2) yields the steady-state continuity equation for $p(x,0^-)$, verifying that (4) is the solution of (2).

Because of quasi-neutrality and low injection, the minority hole diffusion current dominates in determining the response from the quasi-neutral

base. The following matrix describes the density of this current at x = 0 and $x = X_{QNB}$:

$$\begin{bmatrix} I(0,s) - i(0,0^-) \\ I(X_{QNB},s) - i(X_{QNB},0^-) \end{bmatrix} = \frac{eD_p}{L_p^*} \begin{bmatrix} 1 & 1 \\ e^{-X_{QNB}/L_p^*} & e^{X_{QNB}/L_p^*} \end{bmatrix} \begin{bmatrix} M_1 \\ M_2 \end{bmatrix} \qquad (5)$$

where $i(0,0^-)$ and $i(X_{QNB},0^-)$ are the initial values (at $t = 0^-$) of the minority hole diffusion current at $x=0$ and $x=X_{QNB}$. In (5), hole current entering the quasi-neutral base is positive, by definition.

Regarding the minority carrier densities at the two edges as the excitation terms for a system analogous to a linear two-port network of circuit theory, we have the following two-port network matrix from (4) and (5) for the two excitations (densities) and the two responses (currents)

$$\begin{bmatrix} I(0,s) - i(0,0^-)/s \\ I(X_{QNB},s) - i(X_{QNB},0^-)/s \end{bmatrix} = \begin{bmatrix} A_{11} & A_{12} \\ A_{21} & A_{22} \end{bmatrix} \begin{bmatrix} P(0,s) - p(0,0^-)/s \\ P(X_{QNB},s) - p(X_{QNB},0^-)/s \end{bmatrix}, \qquad (6)$$

where $p(0,0^-)$ and $p(X_{QNB},0^-)$ are the initial values of the excess hole densities. Equation (6) extends a similar earlier development [1] by including initial conditions so that transients may be directly studied. We call Eq. (6) the <u>master equation</u> for the quasi-neutral base, and the square A matrix is the <u>characteristic matrix</u> of the base region. In (6), $A_{12}=A_{21}= -e(D_p/L_p^*)\,\mathrm{cosech}(X_{QNB}/L_p^*)$ and and $A_{11} = A_{22} = e(D_p/L_p^*)$. Fig. 1 displays the master equation, where the initial values are included in $I(0,s)$. $-P(X_{QNB},s)$, etc. for compactness of expression.

<u>Transient solutions</u> can be derived from (6) by inserting proper boundary conditions, initial values and constraints imposed by the external circuit.

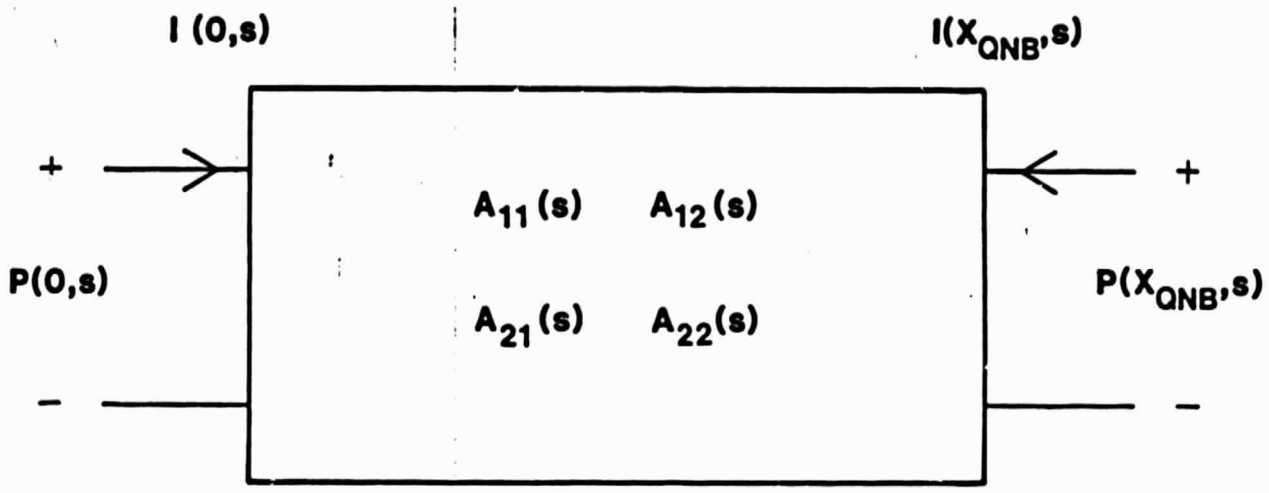

Fig. 1 Two-port network representation for hole density and hole current (density) at the two edges of the n-type quasi-neutral base region.

For example, $I(0,s)=0$ in OCVD open-circuit-voltage-decay [2], $I(0,s)$=constant for reverse step recovery [3], and $P(0,s) = 0$ for short-circuit current decay, the latter of which is developed in detail here.

For small-signal methods [4]-[5], where dI, for example, is an incremental change of current, $I(0,s)=I_{DC}/s + dI(0,s)$ and $P(0,s)=P_{DC}/s + (edV/kT)P_{DC}$. Here the suffix DC denotes a dc steady-state variable. In later sections, we will show briefly how to get solutions from the master equation for various of these methods.

In a solar cell, the back contact system, including the low-high junction, is generally characterized in terms of effective recombination velocity, S_{eff}. The boundary condition at the back contact is $I(X_{QNB},s) = -eS_{eff}P(X_{QNB},s)$. From a circuit viewpoint, this relation is equivalent to terminating Fig. 1 by a resistor of appropriate value dependent partly on S_{eff}. Because S_{eff} in part determines the transient in the various methods named above, we can determine S_{eff} from the transient response, as will be shown.

In the treatment to follow, we consider the utility of the master equation in characterizing selected measurement methods. The main emphasis will be placed on the short-circuit current decay.

Before doing this, however, we shall remark on the simplicity provided by the master equation (Eq. 6) by comparing it with its counterpart in the steady state.

3. TRANSIENT VS. STEADY-STATE ANALYSIS VIA TWO-PORT TECHNIQUES

In general, the current (current density for a unit area) is the sum of the hole current, the electron current and the displacement current. For the quasi-neutral regions under study using the two-port technique described

previously, the displacement current is negligible. In the steady state, the two-port description leading to the master equation simplifies because then the hole current in our example of Sec. 2 depends only on position x. This x-dependence results from volume recombination (relating to the minority-carrier lifetime) and effective surface recombination (relating to the effective surface recombination velocity). A two-port formulation for the steady state leads to the same matrix description as that derived previously, in which the matrix elements $A_{ij}(s)$ of Eq. (6) still hold but with the simplification that $s = 0$. From such a master equation, one can determine the hole current at the two edges of the quasi-neutral base; and, using quasi-neutrality together with knowledge of the steady-state currents in the junction space-charge region and in the p^+ quasi-neutral emitter region, one can thus find the steady-state current flowing in the external circuit or the voltage at the terminals of the diode. If the quasi-neutral base is the principal region of the device, in the sense that it contributes dominantly to the current or voltage at the diode terminals, then one has no need to consider the current components from the other two regions.

In contrast the general time-varying mode of operation leads to a minority hole current in the n-type quasi-neutral base of our example that depends on two independent variables, x and t. The time dependence results because the holes not only recombine within the region and at its surface, but also their number stored within the base varies with time. This may be regarded as resulting from the charging or discharging hole current associated with $\partial p/\partial t$ in the hole continuity equation. This charging or discharging current complicates the variation of the hole current in space and time. But the use of the Laplace transform of the two-port technique in effect reduces the complexity of the differential equation to the level of that describing

the steady state; the dependence on variable t vanishes, reducing the partial differential equation to an ordinary differential equation in x, just as in the steady state.

This comparison also brings out another point. Just as in the steady state, one must interpret the transient voltage and current at the diode terminals as resulting not only from the quasi-neutral base but also from the junction space-charge region and the quasi-neutral emitter. In the interpretation of experiments to follow, we shall discuss complications arising from this multi-regional dependence.

4. OPEN CIRCUIT VOLTAGE DECAY (OCVD) AND REVERSE STEP RECOVERY (RSR)

In OCVD, a widely used method [2], the free carriers in the junction space-charge region enter to contribute to the transient. But, consistently with Sec. 2, and with most common usage, we concentrate at first on the n-type quasi-neutral base.

From the master equation [Eq. (6)], the transient solution for the junction voltage is obtained from open-circuit constraint (for $t > 0$) that $I(0,s)=0$:

$$P(0,s) = p(0,0^-)/s - \frac{i(0,0^-)L_p^*}{eD_p s} \quad \frac{1 + \{D_p[\coth(X_{QNB}/L_p^*)]/L_p^* S_{eff}\}}{\coth(X_{QNB}/L_p^*) + (D_p/L_p^* S_{eff})} \quad . \tag{7}$$

Here we have assumed that the quasi-neutral base is the principal region in the sense described in Sec. 4; that is, we neglect contributions from all the other regions of the device.

Using the Cauchy's residue theorem, we find the inverse transform of Eq. (7):

$$p(0,t) = -\sum_{i=1}^{\infty} \frac{2i(0,0^-)L_p}{eD_p s_i \tau_p} \frac{[1 + (D_p K_i/L_p S_{eff})\cot(X_{QNB}K_i/L_p)]\exp(s_i t)}{[(X_{QNB}/L_p)\mathrm{cosec}^2(X_{QNB}K_i/L_p) + (D_p/L_p S_{eff})]} \tag{8}$$

where s_i is the ith singularity point (ith mode) which satisfies the Eigenvalue equation,

$$\coth(X_{QNB}\sqrt{1+s_i\tau_p}/L_p) + D_p\sqrt{1+s_i\tau_p}/L_p S_{eff} = 0 \tag{9}$$

and $K_i = \sqrt{-1-s_i\tau_p} > 0$, where $s_i < 0$.

As can be seen in Eq. (8), the decay of the excess hole density at x=0 is a sum of exponentials; each Eigenvalue s_i is called a mode, as in the electromagnetic theory. Appendix A treats the details of determining the Eigenvalues s_i from Eq. (9) (and from the similar Eq. (11) derived below).

The decaying time constant $-1/s_1$, of the first mode is much the largest of the modes. Both s_1 and the initial amplitude of the first mode are functions of S_{eff} and τ_p. Thus separating the first mode from the observed junction voltage decay curve, by identifying the linear portion of v(t), will enable, in principle, determination of S_{eff} and τ_p simultaneously. But our recent experience, coupled with that cited in [6], suggests that this is seldom possible in practice for Si devices at T ≃ 300 K. In Si devices the open-voltage decay curve is usually bent up or bent down because of discharging and recombination within the space-charge region.

As mentioned in [4], the mobile charge within the space-charge region contributes significantly to the observed voltage transient for Si, in which

$n_i \sim 10^{10}$ cm^{-3}, but not in Ge, for which OCVD was first developed, and for which $n_i \sim 10^{13}$ cm^{-3}. Here n_i is the intrinsic density and is also the ratio of the pre-exponential factors that govern contributions from the quasi-neutral regions relative to those from the junction space-charge region.

Thus we identify the transient decay of mobile electrons and holes within the p/n junction space-charge region, which persists throughout the open-circuit voltage decay (OCVD), as a mechanism that distors OCVD so significantly that the conventional treatment of OCVD will not reliably determine τ_p or S_{EFF}. The conventional treatment is consistent with that proceeding from the master equation, as described in this section. The interested reader may consult Ref. 4 for experimental comparisons that lead to this conclusion. We shall not pause here to present these.

Rather we shall turn briefly to possible methods to remove the effects of this distortion. In an attempt to characterize the space-charge-region contribution to the observed transient voltage [6], quasi-static approximations and a description of the forward-voltage capacitance of the space-charge region based on the depletion approximation were combined to give rough estimates of this contribution. We plan to refine the approximations and the estimates in a future publication, leading possibly to a variant of OCVD useful for determining τ_p and S_{eff}.

In the reverse step recovery (RSR) method [3], in which again the diode is subjected to steady forward voltage for $t > 0$, we have two constraints (for $t > 0$). The first is $I(0,s)$ = constant (reverse current), $0 < t < \tau_s$, where τ_s is the time needed for the excess hole density $p(0,t)$ to vanish. This is the primary constraint. (The second constraint is $p(0,t) \simeq -n_i^2/N_{DD}$ for $\tau_s < t < \infty$, a result of applied reverse bias through a resistor.)

The primarily observable storage time τ_s is estimated by following a procedure similar to that described in Sec. 4, proceeding from the master equation.

This method suffers difficulties similar to that of the OCVD method. Because $p(0,t) > 0$ for $0 < t < \tau_s$, the decay of mobile hole and electron concentrations in the p/n junction space-charge region complicates the interpretation of the measured τ_s in terms of the desired parameters, τ_p and S_{eff}.

In addition to this, during the portion of recovery transient occuring for $\tau_s < t < \infty$, the reverse generation current is often large enough to saturate the recovery current so quickly that we have no sizable linear portion of the first-mode curve on a plot of $\ln[i(t)]$ vs. t. This linear portion provides interpretable data for Ge devices [3], but not often for Si devices according to our experiments.

We shall not pause here to present experimental evidence, but rather postpone that presentation until a planned future publication where comparison with previous work can be comprehensive.

5. SHORT CIRCUITED CURRENT DECAY (SCCD), A NEW METHOD: PART 1

5.1 Brief Physics and Mathematics

In this method, one first applies a forward bias to set up a steady-state condition and then suddenly applies zero bias through a resistance so small that the constraint is essentially that of a short circuit. Thus, for $t > 0$, the p/n junction space-charge and quasi-neutral regions discharge. One measures the transient current via the voltage across the small resistor. If the discharging time constants related to the charge stored within the quasi-neutral emitter and the junction space-charge region are much smaller than

from the quasi-neutral base, one can separate the first mode of the quasi-neutral-base response and determine S_{eff} and τ_p.

We first consider the time of response of the junction space-charge region. Upon the removal of the forward voltage, the constraint at the terminals becomes essentially that of a short circuit. The majority-carrier quasi-Fermi levels at the two ohmic contacts immediately become coincident, and the junction barrier voltage rises to its height at equilibrium within the order of the dielectric relaxation time of the quasi-neutral regions, times that are of the order of no greater than 10^{-12}s. This occurs because the negative change in the applied forward voltage introduces a deficit of majority holes near the ohmic contact of the p^+ emitter and a deficit of majority electrons near the ohmic contact in the quasi-neutral base. The resulting Coulomb forces cause majority carriers to rush from the edges of the junction barrier regions, thus causing the nearly sudden rise of the barrier height to its equilibrium value. (The physics governing this phenomena comes from Maxwell's Curl $\underline{H} = \underline{i} + \partial\underline{D}/\partial t$; taking the divergence of both sides yields $0 = \text{div}\ \underline{i} + \partial(\text{div}\ \underline{D})/dt$, which, when combined with $\underline{i} = (\sigma\underline{D}/\varepsilon)$ and $\text{div}\underline{D} = \rho$, yields a response of the order of ε/σ, the dielectric relaxation time.)

Following this readjustment of the barrier height, the excess holes and electrons exit the junction space-charge region within a transit time of this region (about 10^{-11}s typically), where they become majority carriers in the quasi-neutral region and thus exit the device within the order of a dielectric relaxation time.

Thus the discharging of excess holes and electrons within the junction space-charge region in the SCCD method occurs within a time of the order of 10^{-11}s, which is much less than any of the times associated with discharge of

the quasi-neutral regions. This absence in effect of excess holes and electrons within the junction space-charge region greatly simplifies the interpretation of the observed transient. It is one of the main advantages of this method of measurement.

A more detailed discussion of the vanishing of excess holes and electrons within the junction space-charge region appears in Appendix B.

The discharge of the quasi-neutral emitter depends on the energy-gap narrowing, the minority carrier mobility and diffusivity, the minority-carrier lifetime, and the effective surface recombination velocity of this region. For many solar cells, this discharge time will be much faster than that of the quasi-neutral base, and we shall assume this is so in the discussion to follow.

Having established that the mobile carriers in the junction space-charge region enter the short-circuit-decay transient during an interval of time too short to be observed, and noting also now that negligible generation or recombination of electrons or holes within this region will occur during the transient, we now turn to the observable transient current. Inserting the constraint, $P(0,s) = 0$, into the master equation, Eq. 6, leads to

$$I(0,s) = i(0,0^-)/s - \frac{eD_p p(0,0^-)}{sL_p^*} \frac{\coth(X_{QNB}/L_p^*) + D_p/L_p^* S_{eff}}{1 + [D_p/L_p^* S_{eff}]\coth(X_{QNB}/L_p^*)} \cdot \tag{10}$$

Cauchy's residue theorem yields the inverse transform of (10):

$$i(t) = -\sum_{i=1}^{\infty} \frac{eD_p p(0,0^-)K_i}{s_i L_p} \frac{\cot(K_i X_{QNB}/L_p) - D_p K_i/L_p S_{eff}}{(\tau_p/2K_i^2) + (X_{QNB}/2S_{eff})\mathrm{cosec}^2(K_i X_{QNB}/L_p)} e^{s_i t} , \tag{11}$$

where s_i is the ith singularity which satisfies the Eigenvalue equation,

$$1 + \frac{D_p}{L_p S_{eff}} \sqrt{1+s_i\tau_p} \coth\left[\frac{X_{QNB}}{L_p}\sqrt{1+s_i\tau_p}\right] = 0 \quad , \tag{12}$$

and where $K_i = (-1-s_i\tau_p)^{1/2} > 0$, with $s_i < 0$.

Truncating (11) and (12) to include only the first mode s_1, we obtain from (11) and (12):

$$1 + (D_p/L_p S_{eff}) \sqrt{1 + s_1\tau_p} \coth[(X_{QNB}/L_p)(1 + s_1\tau_p)^{1/2}] = 0 \tag{13}$$

and

$$i_{\text{first mode}}(0) = - \frac{eD_p p(0,0^-)K_1}{s_1 L_p} \quad \frac{\cot(K_1 X_{QNB}/L_p) - (D_p K_1/L_p S_{eff})}{(\tau_p/2K_1^2) + (X_{QNB}/2S_{eff})[\text{cosec}^2(K_1 X_{QNB}/L_p)]} \quad . \tag{14}$$

Equations (13) and (14) contain four unknowns: $i_{\text{first mode}}(0)$, s_1, τ_p and S_{eff}. The parameters, s_1 and $i_{\text{first mode}}(0)$ are determined from the straight-line portion of the observed decay (in Fig. 3c to be discussed below): $p(0,0^-) = (n_i^2/N_{DD})[\exp(ev(0^-)/kT)-1]$. Here $v(0^-)$ is known from the steady forward voltage applied for $t < 0$ and the doping concentration N_{DD} of the base is measured by usual methods; $D_p(N_{DD})$ is known from the standard tables and X_{QNB} is measured. Combining (14) and (13) then yields the desired parameters: τ_p and S_{eff}.

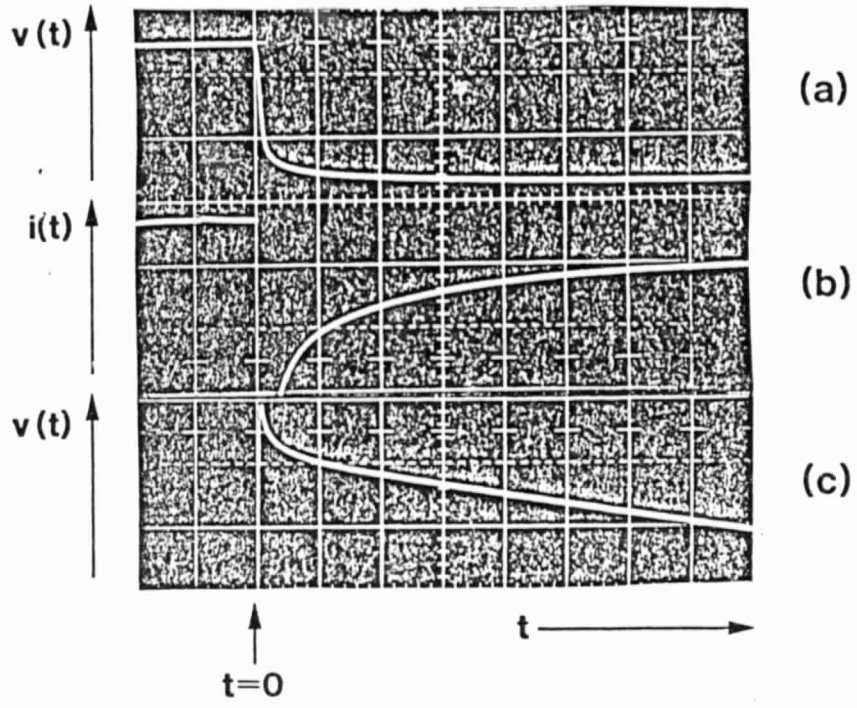

Fig. 3 (a) Voltage across BSF #1 solar cell (vertical:.2V/div).
(b) Current through BSF #1 solar cell (vertical:1mA/div).
(c) Log scale representation of (b) (vertical:.1V/div), where $v(t) = (mkT/e)\log_e[i(t)/I_0 + 1]$.

In (a)-(c), horizontal axis is 10 μs/div.

We measured the voltage across the solar cell under study. As illustrated in Fig. 3(a), the voltage drops by 0.1 V within 1 μs. This means that the excess minority carrier density p(0,t) drops to 2% of its initial value within 1 μs. The speed is circuit limited. One could design a much faster circuit. Here $\tau_d = -1/s_1$ is the first-mode decay time, influenced by both volume and surface recombination in the base. But the circuit used suffices because $\tau_p >> 1$ μs for the solar cells studied. Fig. 3(b) shows the current during the transient. Fig. 3(c) is its semi-logarithmic counterpart, illustrating the straight-line position of the transient obtained from the output of the logarithmic amplifier in Fig. 2. From this τ_d is determined. Since the voltage at node B is purely exponential for a time, the corresponding output voltage at node C is linear in time, as Fig. 3(c) illustrates. We used switching diodes in the log amplifier whose I-V characteristic is $V = .0385 \ln(I/I_o+1)$. If the first-mode current is

$$I_{\text{first-mode}}(t) = \text{constant } \exp(-t/\tau_d) \quad , \quad \tau_d \tilde{=} -1/s_1 \quad , \tag{15}$$

then the slope of the output voltage of log amplifier is $-38.5 \text{ mV}/\tau_d$. Extrapolation of the straight portion in Fig. 3(c) yields the initial value of $i_{\text{first-mode}}(0^+)$ as the intercept.

We measured the decay time constant and the initial amplitude of the first-mode current as follows. For DEVICE 1, $\tau_d \equiv -1/s_1 = 29.3$ μsec, $i_{\text{first-mode}}(0^+) = 2.73$ mA for $v(0^-) = 0.44$ V and T = 303.1 K. For DEVICE 2, $\tau_d = 24.5$ μsec, $i_{\text{first-mode}}(0^+) = 4.35$ mA for $v(0^-) = 0.5$ V and T = 302.9 K. For DEVICE 3, $\tau_d = 28.5$ μsec, $i_{\text{first-mode}}(0^+) = .696$ mA at $v(0^-) = .47$ V and 303.5 K. Here $v(0^-)$ denotes the steady forward voltage applied across the solar cell before transient.

From the above development, these results give: For DEVICE 1, τ_p = 119 μs, S_{eff} = 25 cm/s; for DEVICE 2 = τ_p = 119 μs, S_{eff} = 60 cm/s; for DEVICE 3, τ_p = 213 μs, S_{eff} = 100 cm/s. These results agree favorably with those obtained for the same devices by using the more time-consuming methods detailed in [4] - [5].

5.3 Comparison with Other Methods

Most measurement methods for the determination of the minority-carrier lifetime and the surface recombination velocity of the base region of Si solar cells share a common problem caused by the existence of the sizable number of the mobile carriers within the space-charge-region. These methods, among open-circuit voltage decay and reverse step recovery were originally developed for Ge devices. Silicon has a much larger energy gap E_G than does Ge. Thus the distortion of the measured response by carriers stored in the junction space-charge region is much more pronounced in Si, mathematically because of the role of the intrinsic density n_i discussed in Sec. 6.

If the electronic switch providing the short circuit closes fast enough, the mobile holes and electrons stored for negative time in the junction space-charge region play no role in determining the response of the short-circuit-current decay for the solar cells described earlier. In our experiments, the simple circuit of Fig. 2 had speed limitations, but these limitations did not markedly influence the accuracy of the determined base lifetime and surface recombination velocity for these solar cells (see Sec. 6 for devices for which this circuit must be improved). This lack of influence results because the decay time of the first-mode response, which accounts for vanishing of minority holes both by volume recombination within the quasi-neutral base and effectively by surface recombination, greatly exceeded the time required for

the excess hole density at the base edge of the space-charge region to decrease by two orders of magnitude.

Apart from this potential circuit limitation, which one can overcome by improved circuit design (see Sec. 6), a more basic consideration can limit the accuracy of the short-circuit-current decay (SCCD) method. In general, the current response derives from vanishing of minority carriers not only in the quasi-neutral base but also in the quasi-neutral emitter. For the solar cells explored in this study, the emitter contributes negligibly to the observed response because of the low doping concentration of the base and because of the low-injection conditions for which the response was measured. But for other solar cells or for higher levels of excitation, the recombination current of the quasi-neutral emitter can contribute significantly.

The contribution from the quasi-neutral emitter may be viewed as an opportunity rather than as a limitation. That is, the SCCD method may have utility wider than that treated here. If the quasi-neutral emitter contains excess charge whose decay time dominates in determining the transient observed, in some devices the parameters of the physical electronics of the highly doped and thin quasi-neutral emitter can be explored using SCCD. An example may be a transistor with a thin and highly doped base region or a solar cell having a high open-circuit voltage controlled by the recombination current in the emitter. For such devices, the absence of contributions from carriers in the junction space-charge region becomes a particularly key advantage not offered by either open-circuit voltage decay or step reverse recovery. The SCCD method also may enable parameter determination if high injection in the base prevails. Exploring these possible uses will require fast switching circuits and determination of the existence of a dominant relaxation time from minority carriers in the highly doped emitter.

Note that the SCCD method determines the base lifetime and the effective surface recombination velocity of a BSF solar cell by a single transient measurement. One can easily automate the determination of these parameters from parameters directly measured from the transient by a computer program, and the measurement itself may be automated. This suggests that SCCD may be useful for in-process control in solar-cell manufacturing.

Recall the mathematical formulation of the relevant boundary-value problem that led to a description similar to that of two-port network theory. The advantages of this formulation were only touched upon earlier and only the bare elements of its relation to open-circuit voltage decay and step reverse recovery were developed. Further exploitation to enable systematic development and comparison of small-signal and transient methods for the determination of material parameters of solar cells and other junction devices is treated, in part, in Sec. 6.

6. IMPROVEMENT OF SHORT-CIRCUIT-CURRENT DECAY METHOD FOR DETERMINING τ AND S OF THE QUASI-NEUTRAL BASE, AN IMPROVEMENT: PART 2

In Sec. 5 we have proposed and illustrated a new method for measuring the surface recombination velocity S and the recombination lifetime τ in the quasineutral base of silicon solar cells and solar cells of other semiconductors.

In the short-circuit decay approach, for $t < 0$, a forward voltage has distributed excess holes and electrons through the volume of the solar cell. Then a switch establishes a short circuit across the solar cell at $t = 0$. For $t > 0$, the resulting transient decay is a key observable. The decay results from the recombination of the excess carriers within the volume of the device and at its surfaces.

The short-circuit decay method has an advantage compared with other methods. This follows from the dielectric relaxation and the drifting of excess holes that yields a junction space-charge region (junction transition region) in which practically no excess holes and electrons exist after about 10 ps. have passed after the switch closes. Thus this carrier storage does not distort the transient decay. Such distortion obscures the interpretation of other transient methods for determining S and τ [7].

For germanium, for which most of the commonly used transient methods was developed, the error thus introduced is negligible; the excess carrier storage in the junction transition region for forward voltage is much less than the storage in the quasineutral base region. This is not so for Si or GaAs. The larger energy gaps and smaller intrinsic densities of these materials lead to relatively very large carrier storage in the junction transition region, as compared with that present in Ge devices. Thus the error introduced by this storage for Si solar cells, particularly highly efficient solar cells in which the carrier storage and recombination in the quasineutral base is small, invalidates the conventional transient methods.

6.1 Improvements in the Circuit for the Short-Circuit Current Decay

We have improved the circuit relative to that reported in Sec. 5. An MOSFET switch (Fig. 4) replaces our former more complicated and slower switching circuit (Fig. 3 of Sec. 5). Part (b) of Fig. 4 shows the observables for $t > 0$. These consist of a slope and an intercept. The relevant theory appears in [7].

The circuit of Fig. 4 offers significant advantages. Our previous circuit led to a relatively slow establishment of the short-circuit conditions. For certain solar cells, this made impossible the determination

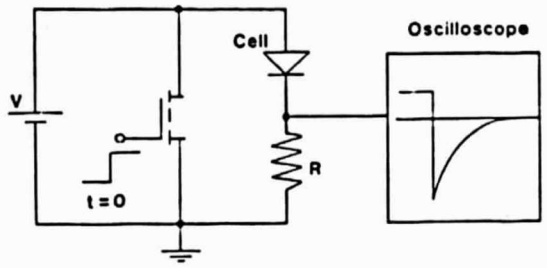

Fig. 4(a) Electronic circuit used in the SCCD method. The switching time of the power MOSFET is less than 100 nsec.

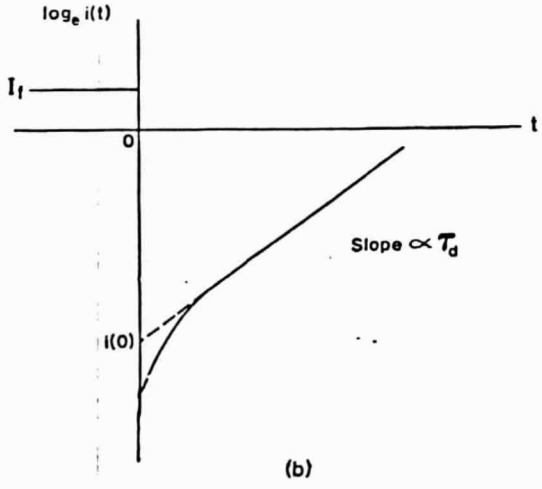

Fig. 4(b) Schematic illustration of the current decay displayed on a log scale.

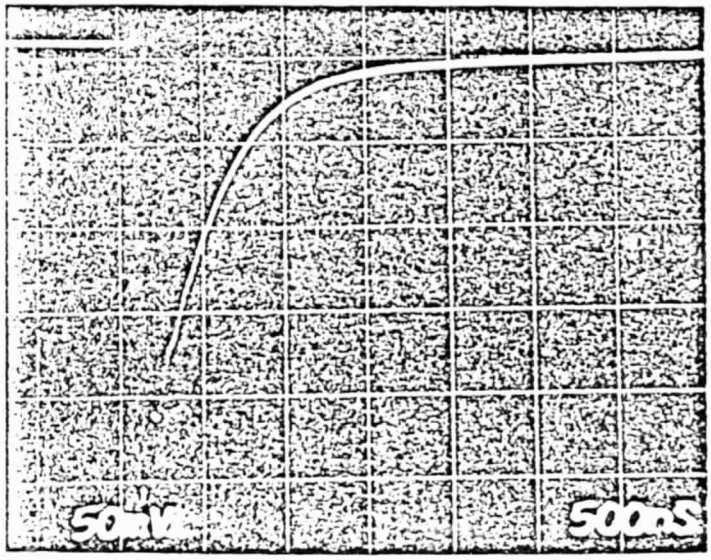

Fig. 4(c) Experimental current decay of a $n^+/p/p^+$ BSF solar cell ($\rho_{base} \simeq$ 0.3 Ωm, $W_{base} \simeq$ 367 μm, $\tau_d \simeq$ 6.4 μsec, $L_n \simeq$ 180 μm, $S_{eff} \simeq$ 1.3×10^3 cm/sec). The vertical scale is 100 mA/division.

of S and τ. The circuit of Fig. 4 switches in approximately 10 ns., and no problems exist in interpreting the lifetime and S of any of the over ten solar cells of different types we have treated.

6.2 Remarks on Sensitivity

Figures 5(a) and (b), developed from theory, illustrate aspects of the sensitivity of the SCCD method. Let L = minority-carrier diffusion length. Let W = quasineutral base thickness. Then for thin cells ($W << L$) the method is sensitive to S because most minority carriers recombine at the back surface. Conversely, for thick cells, $W >> L$, the method is sensitive to τ but not to S.

In the limiting cases just described, the SCCD method will yield only one of the desired parameters, either τ or S. To determine the other parameter requires another measurement that depends both on S and τ (or L). For example, one can use the dark reverse saturation current or the open-circuit voltage. Both of these parameters may be influenced by quasineutral emitter recombination. Thus error can occur. Use of small-signal admittance avoids this error.

6.3 Small-Signal Admittance, Preliminary Remarks

This technique works well as the needed supplement. Neugroschel (1984) has described details of the application of this technique as a supplement to SCCD. This work resulted as part of an ongoing collaboration between the present Principle Investigator and Professor Neugroschel. Graduate Research Student, T. W. Jung, is continuing these efforts. We describe the method and its results in Sec. 7.

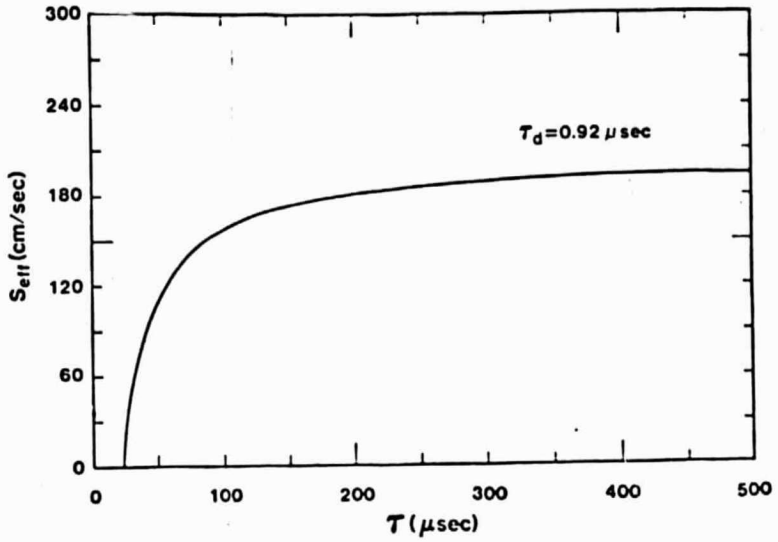

(a)

Fig. 5 (a) Plot of S_{eff} vs τ for a thin $n^+/p/p^+$ BSF solar cell ($\rho_{base} \simeq 10$ Ωcm, $W_{base} \simeq 92$ μm).

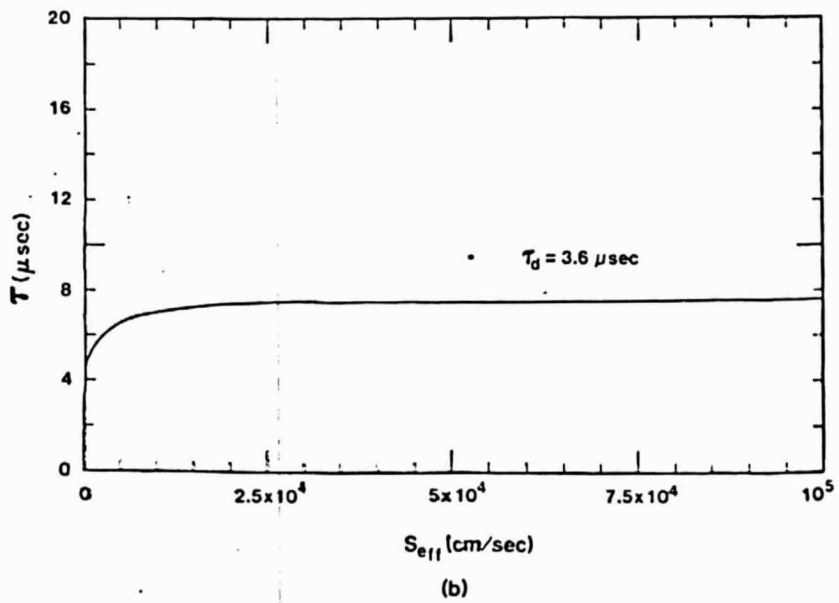

(b) Plot of τ vs S_{eff} for a thick $n^+/p/p^+$ BSF solar cell ($\rho_{base} \simeq 0.15$ Ωcm, $W_{base} \simeq 295$ μm).

Table 1: Summary of results for some typical solar cells. The values for L_{base} and S_{eff} were obtained using the SSCD method, unless marked otherwise

CELL	ρ_{base} (Ωcm)	W_{base} (μm)	L_{base} (μm)	S_{eff} (cm/sec)
$n^+/p/p^+$	10	227	454	105
BSF			450*	
$n^+/p/p^+$	10	103	250	2.9×10^3
BSF				
$n^+/p/p^+$	10	360	512	2×10^5
$n^+/p/p^+$	0.15	295	100	---
$p^+/n/n^+$	10	320	80$^+$	503*
BSF				500†
$n^+/p/p^+$	10	92	~600*	~180
BSF				

* obtained from G_{QN}^{HF}

† obtained from G_{QN}^{LF}

6.4 Representative Results

These appear in Table 1. Although over ten different solar cells were measured using SCCD, we report six here, relegating further reporting to the future when the detailed physical make-up of the solar cells becomes available.

7. SMALL-SIGNAL ADMITTANCE MEASUREMENTS [9-11]

Small-signal admittance measurements can be used to analyze a variety of semiconductor devices. We discuss here specifically the applications for analyzing the solar cells, namely measurement of the base L and S_{eff} and the separation of the emitter and the base current components. The small-signal measurements can be performed either at low-frequencies ($\omega\tau << 1$) or high frequencies ($\omega\tau >> 1$). The choice of a particular frequency range will depend on the W/L ratio.

7.1 Low-frequency method (LF) [9,10]

Consider a $n^+/p/p^+$ BSF solar cell shown in Fig. 6(a). For a low-frequency signal with $\omega\tau_n << 1$, where τ_n is the minority-carrier electron lifetime in the p-type base, we derive the expressions for the small-signal quasi-neutral base capacitance C_{QNB}^{LF} and conductance G_{QNB}^{LF}, respectively (see equations (D1) and (D2) in Appendix D). Equations (D1) and (D2) contain four unknowns: C_{QNB}^{LF}, G_{QNB}^{LF}, L_n, and S_{eff}. The parameters C_{QNB}^{LF} and G_{QNB}^{LF} are measured and the combination of (D1) and (D2) yields L_n and S_{eff}.

It is worthwhile to discuss in more detail a few special cases:

7.1.1 Long diode: W > L

For this case, (D1) and (D2) yield a simple expression for C_{QNB}^{LF} and τ_n

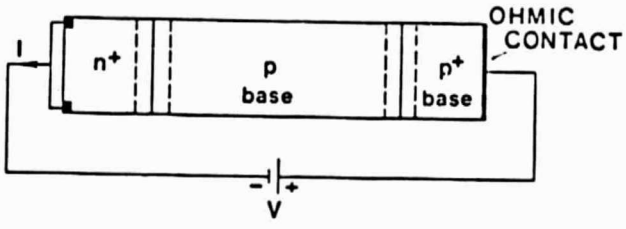

(a)

Fig. 6 (a) Schematic diagram of an $n^+/p/p^+$ BSF solar cell.

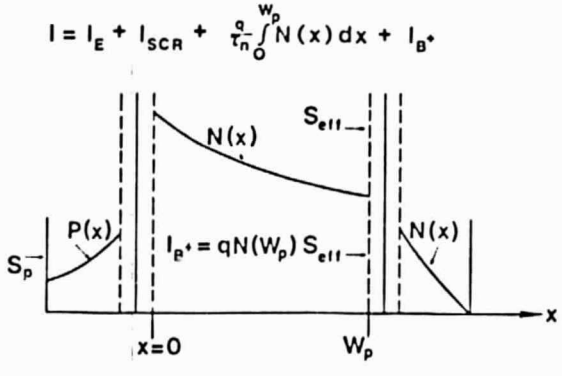

(b)

(b) Qualitative sketches of minority-carrier distributions in the dark.

$$C_{QNB}^{LF} = \frac{q}{kT} \frac{Aqn_i^2 L_n}{2N_{AA}} \left[\exp\left(\frac{qV}{kT}\right) - 1\right] \qquad (16)$$

and

$$\tau_n = \frac{2C_{QNB}^{LF}}{G_{QNB}^{LF}} \quad . \qquad (17)$$

The base diffusion length is obtained either from (2) or from (3). Thus $L_n^2 = D_n \tau_n$ and τ_n are determined independently. The details concerning the deduction of C_{QNB}^{LF} and G_{QNB}^{LF} from the data are discussed in [9]. As an illustrative example, we show in Fig. 7 the measured $C_{QNB}^{LF}(V)$ and $G_{QNB}^{LF}(V)$ plots for the p^+/n device with $N_{DD} = 1.25 \times 10^{15} cm^{-3}$. The analysis using (16) or (17) gives $L_p = 80$ μm. Note that n_i^2 does not enter Eq. (17). Thus the determination of τ_n is independent of energy-gap narrowing.

7.1.2 BSF solar cell: $W_p \lesssim L_n$, $W_p D_n / L_n^2 < S_{eff} < (D_n\ W_p)$

In this case, (D1) and (D2) are solved to yield L_n and S_{eff}. Figure 8 shows the measured C(V) and G(V) dependencies for a $p^+/n/n^+$ BSF solar cell from which we derive $L_p \simeq 500$ μm and $S_{eff} \simeq 80$ cm/sec.

The method fails, however, for $S_{eff} \ll D_p\ W/L_n^2$; in this case $G_{QNB}^{LF} \simeq KW_p/\tau_n$ yields τ_n, but S_{eff} cannot be found. Another limitation exists for high values of $S_{eff} \gg D_n/W_p$: in this case both (D1) and (D2) are independent of L_n and S_{eff}.

The above difficulties with the LF method can be largely eliminated by the high-frequency approach.

7.2 High-frequency method (HF) [11]

We treat the high frequency method for two special cases.

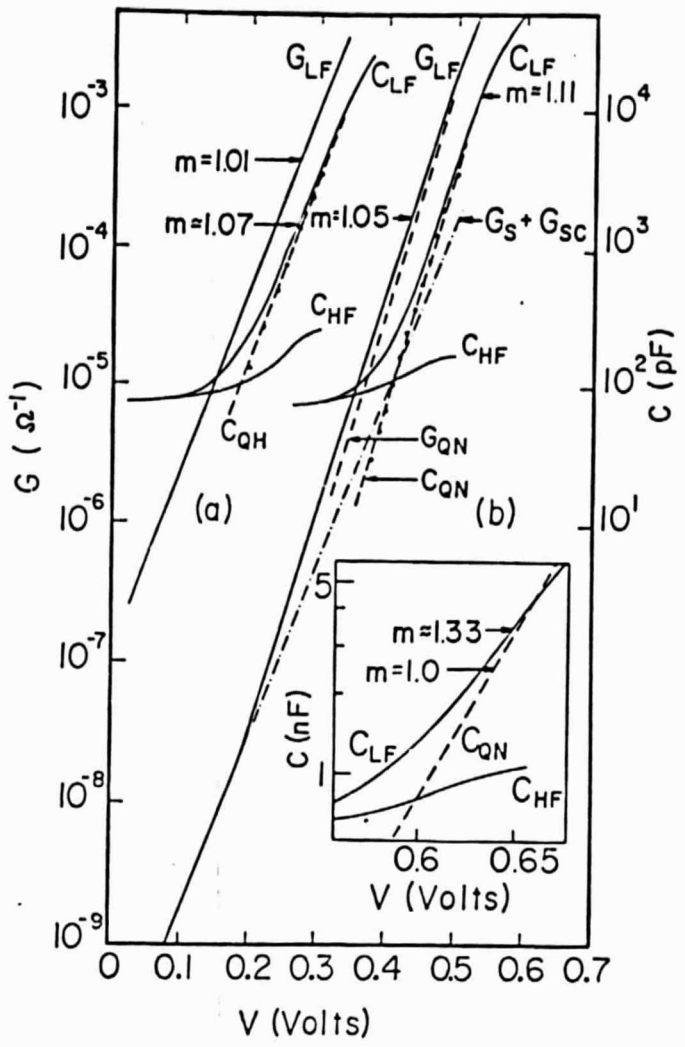

Fig. 7 Measured conductance and capacitance vs. forward-bias V for a long p^+/n diode with $N_{DD} = 1.25 \times 10^{15}$ cm^{-3} and $W_{base} \approx 250$ μm (from Ref. [9]).

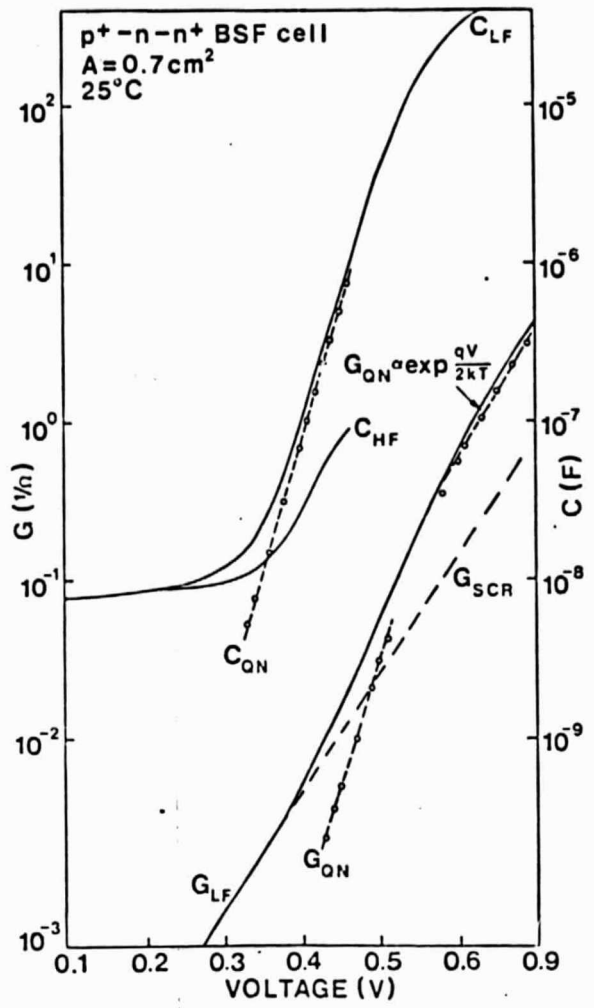

Fig. 8 Measured capacitance and conductance vs forward bias for a $p^+/n/n^+$ BSF solar cell (from Ref. [10]). Here, $N_{DD} \simeq 6 \times 10^{14}$ cm^{-3}, $W_{base} \simeq 320$ μm.

7.2.1 $\omega\tau_n > 10$ and $0.1 \lesssim W_p/L_n \lesssim 1$

The small-signal admittance then is

$$Y_{QNB}^{HF} \simeq \frac{KD_n}{L_n}\left[\left(\frac{\omega\tau_n}{2}\right)^{1/2} + j\omega\left(\frac{\tau_n}{2\omega}\right)^{1/2}\right] = G_{QHB}^{HF} + j\omega\, C_{QNB}^{HF} \quad . \tag{18}$$

The important conclusion from (18) is that the $\omega^{1/2}$ dependence gives the range of $0.1 \lesssim W_p/L_n \lesssim 1$ regardless of the value of S_{eff}. To obtain the desirable parameters, we measure G_{QNB}^{HF} vs ω for $\omega\tau > 10$ and extrapolate to lower frequencies to obtain an intercept ω_I with G_{QNB}^{LF} given by (D2). This gives

$$L_n^2 = \left(\frac{2\, W_p^2\, D_n}{\omega_I}\right)^{1/2} \left(\frac{D_n}{W_p}\right) \frac{1 + (S_{eff}L_n^2/D_nW_p)}{(D_n/W_p) + S_{eff}} \tag{19}$$

Note again that n_i^2 does not enter. Equation (19) cannot be be solved for L_n and S_{eff} except for the following cases:

a) $S_{eff} < D_nW_p/L_n^2 < D_n/W_p$

$$L_n \simeq (2W_p^2 2D_n/\omega_I)^{1/4} \tag{20}$$

b) $D_nW/L_n^2 < S_{eff} < D_n/W_p$

$$S_{eff} \simeq (\omega_I D_n/2)^{1/2} \quad . \tag{21}$$

The method is illustrated in Fig. 9 for the $p^+/n/n^+$ solar cell of Fig. 8. G_{QN}^{HF} follows the $\omega^{1/2}$ dependence for $f \gtrsim 10^4$ Hz with the intercept at ω_I =

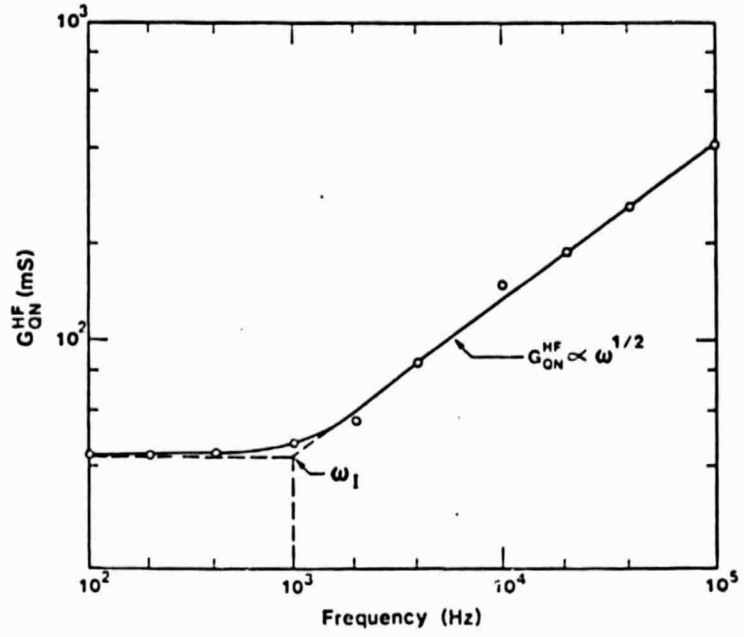

Fig. 9 Measured high frequency conductance G_{ON}^{HF} vs freqency for the $p^+/n/n^+$ solar cell of Fig. 8. The conductance was measured at forward bias V = 0.5 V and shows $\omega^{1/2}$ dependence.

$(2\pi)10^3$ 1/sec. Using (19) and combining with $S_{eff} \approx 80$ cm/sec obtained by the LF method, we have $L_p \approx 503$ μm, which is in excellent agreement with $L_p \approx 500$ μm using the LF method alone.

Even though the general solution (19) cannot give L and S_{eff} exactly, and only one of the parameters is obtained either from (20) or from (21), the method is very useful because: (i) the G_{QN}^{HF} vs $\omega^{1/2}$ dependence shows that $L > W$; (ii) the G_{QN}^{HF} vs $\omega^{1/2}$ dependence indicates that the emitter contribution to the conductance (and dark current) is negligible (this point is discussed further below); (iii) the SSCD for $L > W$ yields an accurate value of S_{eff} only and using this value in (19) we obtain an accurate value for L. The combination of these two methods gives L and S_{eff} for practically any cell.

The sensitivity of the HF method to the emitter component G_{QNE}^{HF} of the total measured quasi-neutral conductance $G_{QN}^{HF} = G_{QNB}^{HF} + G_{QNE}^{HF}$ is explored in Fig. 10. The time constant τ_E of G_{QNE}^{HF} is given by either the Auger lifetime τ_A in the heavily doped emitter, or by the combination of τ_A and the transit time [12]. The emitter time constant is much shorter than the base lifetime, thus G_{QNE}^{HF} is frequency independent up to $f \approx 1/\tau_E >> 1/\tau_B$. Figure 10 shows $G_{QN}^{HF} = G_{QNB}^{HF} + G_{QNE}^{HF}$ for an arbitrary choice of $G_{QNE}^{HF}/G_{QNB}^{HF}$. The region far away from the knee can be fitted to a straight line with $G \propto \omega^{1/m}$, where $m > 2$. Notice, however, that ω_I for $G_{QNE}^{HF} > 0$ is close to the intercept value ω_I for $G_{QNE}^{HF} = 0$. Furthermore, since $L \propto \omega_I^{1/4}$, a small error in ω_I gives only a negligible error in L. For example, for $G_{QNE}^{HF} = G_{QNB}^{HF}$, $\omega_I \approx 1.5\ \omega_I$ ($G_{QNE}^{HF} = 0$), this gives an error in L of only about 10%.

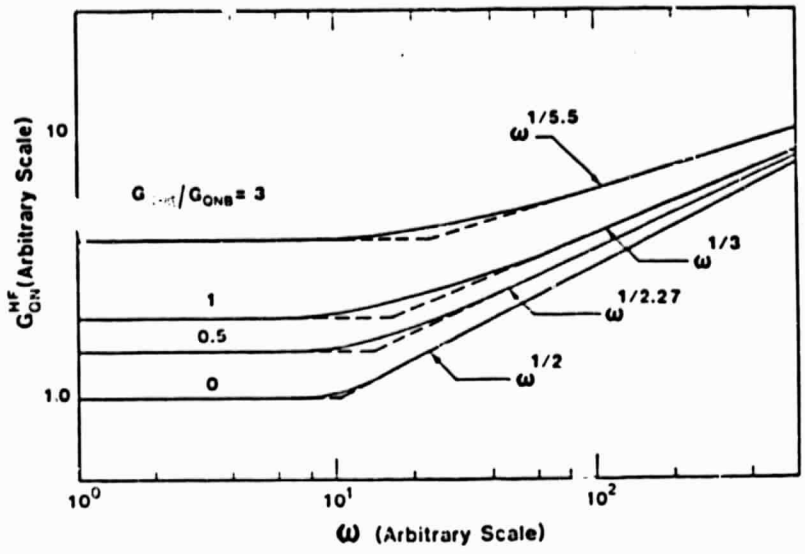

Fig. 10 Plot of $G_{QN}^{HF} = G_{QNB}^{HF} + G_{QNE}^{HF}$ for different ratios of $G_{QNE}^{HF}/G_{QNB}^{HF}$ = 0, 0.5, 1, 3.

7.2.2 $\omega\tau_n > 10$, $W_p/L_n \leq 0.1$

The condition $W_p/L_n \leq 0.1$ may apply for the thin cells (50 - 100 μm) with a very long lifetime. For this case we have

$$G_{QN}^{HF} \simeq KD_n \frac{(\omega^2 W_p^3/3) + S_{eff}(D_n + S_{eff}W_p)}{(D_n + S_{eff}W_p)^2} \quad . \tag{22}$$

For BSF cells, $S_{eff} < D_n/W_p$ and (22) yields

$$G_{QN}^{HF} \simeq K[\omega^2(W^3/3D_n) + S_{eff}] \quad . \tag{23}$$

Figure 11 shows the G_{QN}^{HF} vs ω dependence for a 8 μm thick epitaxial n-type layer with doping density $N_{DD} = 5 \times 10^{15}$ cm^{-3}. The ω^2 dependence for $f > 1.5$ MHz immediately gives $L_p > 10W > 80$ μm and also $S_{eff} << \omega^2W^3/3D_n << 1.2 \times 10^3$ cm/sec. More accurate analysis of the knee region below the ω^2 dependence gives $S_{eff} \simeq 120$ cm/sec and using this value in (B1) gives more accurate $L_p \simeq 90$ μm.

Note, that the HF method for $L > 10\ W$ gives only the lower limit of L and the upper limit of S_{eff}. A combination of this technique with either the LF method or the SCCD can give more accurate results.

7.2.3 $\omega\tau_n \sim 10$, $W_p/L_n \sim 0.1$

For the previous two special cases we have obtained $G_{QNB}^{HF} \propto \omega^{1/2}$ for $W_p/L_n \lesssim 0.1$ and $G_{QNB}^{HF} \propto \omega^2$ for $W_p/L_n \lesssim 0.1$. Obviously, there has to be an intermediate range for $W_p/L_n \sim 0.1$ where $G_{QNB}^{HF} \propto \omega^m$ ($< m \lesssim 2$). One possible approach here is to obtain S_{eff} from the SCCD method and then fit the theoretical $G_{QN}^{HF}(S_{eff}, L_n)$ with the experiment. A very reasonable

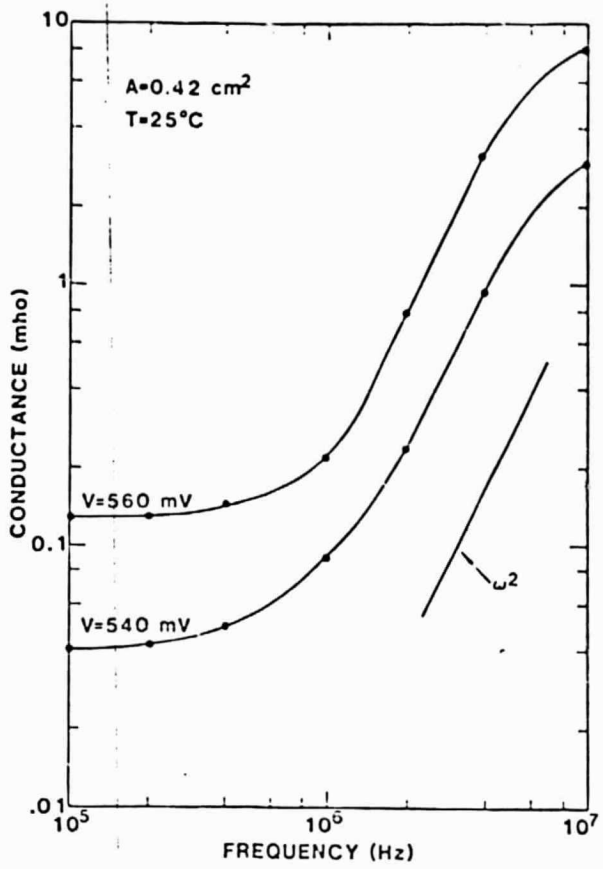

Fig. 11 Frequency dependence of high-frequency conductance for a thin (8 μm) n-type epitaxial layer (from Ref. [5]). The conductance follows ω^2 dependence.

approximation of τ_n can be made, however, by realizing that the G_{QN} vs ω dependence begins to increase from its low-frequency value for $\omega = \omega_I \approx 10/\tau_n$ [11]. Thus, $\tau_n \approx 10/\omega_I$, where ω_I can be approximated as the intercept of the G_{QN}^{LF} line with the extrapolated $G_{QN}^{HF} \propto \omega^m$ dependence.

7.2.4 Interpretation by Analogy.

The mathematical descriptions given above indicate that the measurements of Y(jw) can yield lifetime τ even though the thickness $W \ll [D\tau]^{1/2}$. But these descriptions do not fully explain this result from the viewpoint of physical reasoning.

Analogy can help provide understanding of the relevant physics. Consider an RC transmission line having resistance r and capacitance c per unit length. Suppose the transmission line has no dissipative loss in parallel with the distributed (resistive) capacitance. Then, if v(x,t) denotes the electric potential and i(x,t) the current on the line, the describing partial differential equations are:

$$\frac{\partial^2 v(x,t)}{\partial x^2} = rc\,\frac{\partial v(x,t)}{\partial t} \quad ; \quad \frac{\partial^2 i(x,t)}{\partial x^2} = rc\,\frac{\partial i(x,t)}{\partial t} \quad . \qquad (24)$$

Using the connections, $v(x,t) \rightarrow n(s,t)$ and $rc \rightarrow 1/D_n$, we see that Eq. (24) is analogous to the continuity equation for the p-type quasineutral base region of a solar cell in low injection provided the lifetime $\tau \rightarrow \infty$. Via this analogy, we shall now discuss the dependence on ω of the effective thickness of the transmission line (or the quasineutral base).

We subject Eq. (24) to Laplace transformation with respect to t ($v,(x,t) \rightarrow V(x,s)$, $i(x,t) = I(x,s)$) and solve the resulting ordinary differential equations. This yields, for example,

$$I(x,s) = A \exp[x\sqrt{src}] + B \exp[-x\sqrt{src}] \qquad (25)$$

where s is the complex frequency variable: $s = \sigma + j\omega$. The integration constants A and B are determined by the boundary conditions, which involve V(x,s), and a two-port formulation results, similar to that described in Sec. 2. This two-port description provide a convenient vehicle for quantitative description.

Now consider, for example, the rc transmission line connected to a voltage source $V_1(s)$ at the left port and disconnected (open-circuited) at the right port where the voltage is $V_2(s)$ Consider the transfer ratio $V_2(s)/V_1(s)$ for the case $s \to j\omega$. Qualitatively we see that the transmission line is a low-pass filter. Thus as ω approaches 0 we anticipate that the transfer ratio will approach unity, and for large ω, we anticipate that the transfer ratio will approach zero. To see the meaning of large ω, we calculate the frequency for which the magnitude of the transfer ratio equals 0.707; this is the so-called cutoff frequency for which the ratio is 3 dbs. below its low-frequency value. (By definition the number of decibels = 10 $\log|V_2/V_1|^2$.).

The two-port formulation mentioned above quickly yields the required condition:

$$|\text{sech}L\sqrt{j\omega_0 rc}| = 0.707 \qquad (26)$$

where ω_0 is the cutoff frequency. From this it follows that

$$\omega_0 = 2.43/[(Lr)(Lc)] \qquad (27)$$

in which the denominator is the product of the total resistance and the total capacitance of the transmission line. Use of the analogy between the transmission line and the quasineutral base region of thickness W yields

$$\omega_0 = 2.43\ D_n/W^2 \tag{28}$$

which is the reciprocal of the transit time across the quasineutral base of thickness W when $\tau \to \infty$. (The more commonly seen expression in which 2 replaces 2.43 is the quasi-static approximation for the transit time).

Thus when the signal frequency applied to the rc transmission line, or to the analogous quasi-neutral base region, equals the reciprocal of the transit time, then the signal reaching the output port of the transmission line, or the back surface of the quasineutral base, falls 3 dbs below its low-frequency value. For the quasineutral base, this implies that the interplay of minority electron diffusion and storage distributed through this region confines the input signal partially within the base region, even for the limiting condition that $\tau \to \infty$ and $S = 0$. Hence we see qualitatively that application of a signal of the form $\exp(j\omega t)$ enables determination of τ, when τ is finite and large in the sense that the time-invariant condition $W << \sqrt{D\tau}$ holds. This is what we set out to demonstrate.

To this point we have treated (24) as an anology. In fact, it is an exact description for low injection conditions in the quasi-neutral base if we regard $v(x,t)$ to be the electrochemical potential (quasi-Fermi potential) for the minority electrons and if we identify, as before, that $r_c \to 1/D_n$. That is, the rc transmission line exactly describes the quasineutral base for the conditions stipulated and for $\tau = \infty$. For finite τ one needs to add a

conductance in parallel with the distributed capacitance to attain a full network representation of the minority-electron transmission line. Sah bases his numerical solutions for solar cells and other semiconductor devices on generalizations of such transmission lines, the most complete versions of which appear in a 1971 paper [8].

7.3 Regional Analysis of Solar Cells

It is important to analyze the contributions of each region of the cell to the total dark current (or V_{oc}). Such an analysis is demonstrated here for a $n^+/p/p^+$ BSF solar cell shown in Fig. 6(b). The analysis is based on the determination of the base parameters τ_n and S_{eff} by one of the methods discussed earlier. This is sufficient to calculate the profile of the minority electrons in the base. The recombination losses in the base are given by (D2) and the recombination losses in the p^+-BSF portion of the base are

$$I_n(W_p) \simeq I_B^+ = AqS_{eff}N(W_p) \quad . \tag{29}$$

The space-charge region (SCR) recombination current I_{SCR} can be determined graphically [12] and the emitter contribution I_E is obtained by realizing that the total dark current is

$$I_D = I_E + I_{SCR} + I_B + I_B^+ \quad . \tag{30}$$

For example, such an analysis of the $p^+/n/n^+$ BSF cell of Fig. 5 gave [10]: $L_p \simeq 500\ \mu m$, $S_{eff} \simeq 80$ cm/sec, $I_B \simeq 0.8\ I_D$, $I_{SCR} \simeq 0.2\ I_D$, $I_E \ll I_D$, $I_B^+ \ll I_D$.

8. COMBINED SCCD AND SMALL SIGNAL ADMITTANCE

Table 1 repeats the summary of results for a number of different cells. A comparison of results obtained by different methods, shown for some cells, demonstrates very good agreement. Notice, in particular, the last cell in Table I, which is a thin cell (W_{base} - 92 μm) with $L_n >> W_B$. For this cell, the SCCD method gives $S_{eff} \approx 180$ cm/sec, but the method is insensitive to L_n (see Fig. 5(a)). We have to combine the SCCD method with the high-frequency small-signal admittance method and then use (19) with S_{eff} obtained from the SCCD method to determine L_n.

The main conclusion of this study is that the SCCD method and the small-signal admittance methods yield a rapid and reliable determination of the base parameters. They also allow the determination of the relative importance of the base and the emitter regions with regard to cell efficiency. Identification of the region limiting the efficiency is a key to an informed cell design.

9. POLYSILICON/SILICON HETEROJUNCTIONS APPLIED TO SOLAR CELLS

Replacement in Si bipolar junction transitor of the metal emitter contact by a highly doped polysilicon layer improves the common-emitter current gain of bipolar transistors. The principal investigator has reviewed some twenty papers dealing with this issue, prominent among which are [14], [15], [16], and [17]. According to de Graaff and de Groot (1979) and to Green and Godfrey (1983), this replacement can lead to common emitter current gain $\beta \approx 100$ in the traditional metal-contact bipolar transistor.

This ten-fold increase in β corresponds directly to a ten-fold decrease of the recombination current in the n^+ emitter. Thus arises the implications for solar cells. The ten-fold decrease can only come from the presence of an

defective surface recombination velocity S at the $n^+Si/n^+polySi$ interface. Recent work by NEUGROSCHEL (1984), outlined below, helped to some degree by the principal investigator, resulted in the conclusion indicated below concerning S.

The physical mechanisms responsible for the decrease in S are complicated by a lack of knowledge of the minority-carrier diffusivity in both the n^+ monoSi and polySi, and by a poor present understanding of the interfacial layer. The parameters of this layer are highly sensitive to fabrication conditions and to surface treatment before the CVD process of polysilicon deposition. Various investigators have explored the chemistry of the interface, where peaks in P or As can occur, where deep-level impurities and interstitial oxygen may occur, and a thin insulating interfacial layer can be created by thermal oxidation or chemical treatments before CVD deposition.

But one thing is clear. The polysilicon/silicon heterojunction acts as an effective surface passivant, reducing recombination losses. Various investigations suggest strongly that the ability to passivate persists in the presence of sunlight.

Several possibilities exist for exploiting this passivant for Si solar cells. Details about these possibilities appear in the recent proposal to JPL by the author.

We now sketch the measurement of S mentioned above. Consider an $n^+polySi/n^+Si/p/n$ bipolar transistor. The n^+ Si emitter has a thickness of $2x10^{-5}$ cm and a position independent doping concentration $\sim 10^{19}$ As atoms/cm^3. The n^+ polySi has a doping concentration of $5x10^{20}$ As atoms/cm^3, determined by SIMS, and a thickness exceeding 300 A. On control samples the n^+polySi is omitted; an ohmic contact is made to the n^+Si. In the forward-active mode, the transistor shows a pre-exponential collector current of 10^{-10} A/cm^2 (± a

factor of 2) on six samples and six controls, deriving from minority-electron injection into a base region having an impurity concentration ~10^{18} boron atoms/cm^3. The base current and its pre-exponential factor, J_{BO} is also measured.

Because J_{BO} derives almost entirely from holes injected into the n^+ emitter, we solve the minority hole continuity equation for this region. This yields J_{BO} as a function of hyperbolic trigonometric functions having arguments involving the following characteristic velocities:

(a) D_E/W_E = diffusion velocity,

(b) W_E/τ_E = volume recombination velocity,

(c) S = surface recombination velocity at the n^+polySi/n^+Si interface.

A standard expansion then yields

$$J_{BO} \simeq (en_i^2/N_{eff})[(D_E/W_E)^{-1} + S^{-1}]^{-1}[1 + (\tau_t/\tau_E)] \quad . \tag{31}$$

Here N_{eff} is the effective concentration in the n^+Si, which takes into account Fermi statistics and energy-gap narrowing according to the experimental study of Neugroschel, Lindholm and Pao [18] and consistent with the theoretical model of Landsberg, Neugroschel, Lindholm and Sah [19]. The result is subject to the assumption of a parabolic quantum density of states as suggested by the experimental considerations of Keyes [20]-[21] and of Shibib and Lindholm [22]. Here also τ_t is the transit time for minority holes in the emitter

$$\tau_t/\tau_E = (W_E^2/2D_E\tau_E) + (W_E/S\tau_E) \quad . \tag{32}$$

If we make the approximation, $\tau_E \simeq \tau$(Auger), then

$$1 + (\tau_t/\tau_E) \simeq 1 + W_E/\tau(\text{Auger})[(W_E/2D_E) + (1/S)$$

$$\simeq 1 + 400\{10^{-5} + 1/S\} \qquad (33)$$

$$\simeq 1,$$

if $S >> 400$ cm/s, a conclusion that still holds if $\tau_E < \tau(\text{Auger})$.

Thus,

$$J_{BO}(\text{poly}) \simeq f_1(D_E/W_E, S) \qquad (34)$$

and

$$J_{BO}(\Omega) \simeq f_2(D_E/W_E) \qquad (35)$$

where $J_{BO}(\Omega)$ denotes the pre-exponential current density when an ohmic contact replaces the polysilicon. From the foregoing,

$$S \simeq (D_E/W_E)\{[J_{BO}(\Omega)/J_B(\text{poly})]-1\}^{-1} \quad . \qquad (36)$$

From the measured performance

$$S \simeq 5000 \text{ cm/s}.$$

Thus the polySi/N^+Si interface provides an ohmic contact for majority electrons but a recombination velocity about <u>three orders of magnitude less than an ohmic contact</u> for the minority holes. This supplies ample incentive to investigate such heterojunction contacts for solar cells.

10. RECOMMENDATIONS AND CONCLUSIONS

The short-circuit current decay method is apparently the only reliable transient electrical method for determining τ and S for a wide variety of Si solar cells. For very thin or very thick devices, this method must be supplemented. Otherwise only τ or only S can be determined accurately, not both. The small-signal admittance method appears to fill this need. Our continuing work will explore this issue more fully.

As recommendations, we offer the following:

(a) Other laboratories, inlcuding JPL, would benefit by setting up the SCCD method.

(b) The open-circuit voltage decay needs development for use in connection with manufacturing lines (see quarterly 2). This requires implementation of expressions for junction capacitance under forward voltage. These have been developed under this contract support, but are not yet written fully.

(c) Measurement of the lifetime and the front surface recombination velocity of the quasineutral emitter is essential. An extension of the admittance methods used here may enable such measurements.

(d) The polysilicon/silicon heterojunction has demonstrated properties desirable enough to warrant investigation about its use in solar cells.

APPENDIX A

Although there are several ways to treat the sudden application of a short circuit replacing forward bias V, perhaps the simplest is to think of voltage -V being applied in series with V at t=0. This treatment emphasizes the change in voltage that starts the ensuing transient. See Fig. A-1(a), below.

Thus at t = 0, this change in voltage raises the right ohmic contact by magnitude eV relative to the left ohmic contact because the ohmic contacts are in equilibrium with the adjoining semiconductor in the sense that the distance between the quasi-Fermi level of majority carriers and the majority-carrier band edge remains the same as in equilibrium. They are in non-equilibrium in the sense that charge carriers can pass through the contacts. At $t = 0^+$, some arbitrarily small time after the application of the short circuit, the change in applied voltage has caused electrons to exit the n-type material adjacent to the contact, leaving behind unbared donor atoms and the positive charge shown in Fig. A-1(b). Similarly holes exit the p-type material (electrons enter the valence band from the metal), giving rise to the negative charge shown in Fig. A.1(b). A near delta function of current i(t), flowing in the direction shown in Fig. A.1(a), establishes this charge configuration at $t = 0^+$. Note that i(t) during the entire transient for $t > 0$ flows in a direction opposite to that occuring for negative time because the transient results in removing the electrons and hole present under forward V.

Having established the existence of this negative charge, we now consider what happens subsequently. Here enters a result developed earlier from operating on Maxwell's equation by the divergence operator:

$$0 = \text{div curl } H = \text{div } j_N + \text{div } j_p + \text{div}[\partial(\varepsilon E)/\partial t] \quad . \qquad (A.1)$$

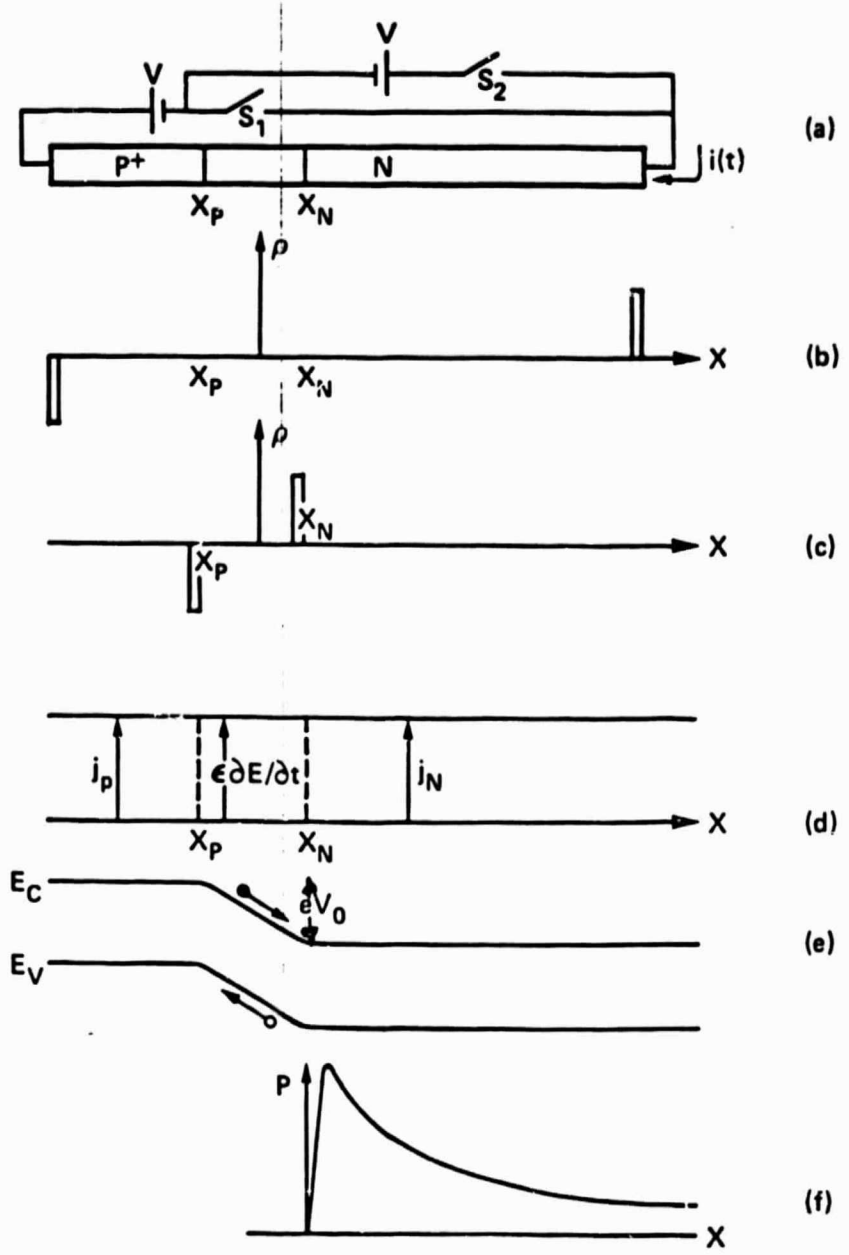

Figure A-1

(a) For $t < 0$, switch S_1 is closed, S_2 is open; conversely for $t > 0$; the junction space-charge region is defined by $x_p < x < x_N$. (b) charge density at $t = 0^+$. (c) charge density for t of the order of a dielectric relaxation time. (d) the total current is x-independent but is essentially majority-carrier convection current in the two quasi-neutral regions and is displacement current in the space-charge region for t of the order of a dielectric relaxation time. (e) electrons and holes drift out of the space-charge region in a transit time. (f) the resulting excess hole density in the space-charge region after a transit time has lapsed.

From this result, two consequences emerge: (1) the charges in Fig. A-1(b) redistribute to the positions shown in Fig. A-1(c) within the order of a dielectric relaxation time $\tau = \varepsilon/\sigma$; and (2) the total current is solenoidal, that is, its divergence is zero, where here the total current includes the displacement current.

The consequence of (2) is illustrated in Fig. A-1(d) for a particular time of order of τ. Notice the large time-rate of change of electric field E within the junction space-charge region, $x_p < x < x_N$. Here we have employed a one-dimensional model so that the operator div becomes the operator $\partial/\partial x$. Thus we see that the electric field in the space charge region grows rapidly so that within t of the order of τ the barrier height has returned to its near equilibrium value and the electric field is several times larger than it was in negative time. But in negative time, the drift and diffusion tendencies of the junction space-charge region were perturbed only by perhaps one part in 10^4 in the forward voltage steady state; that is, the space-charge region was in quasi-equilibrium. For t of the order of τ, the drift tendency now overwhelms the diffusion tendency, and holes and electrons drift out of the space charge region in a transit time τ' determined by $x_N - x_p$/velocity where the velocity approaches the scatter limited velocity because of the high field (Fig. A-1(e)). For typical devices, τ' will be of the order of 10^{-11} s. After this time has passed, the hole and electron concentrations will have returned nearly to their equilibrium values.

Because 10^{-11} s is a time not observed by typical measurement equipment, we think of the initial condition established by shorting the terminals suddenly as that of quasi-neutral regions still storing

approximately the same excess charge as was present in the steady state of negative time, of a space-charge region at the equilibrium barrier height and devoid of excess holes and electrons, and as an excess minority carrier density in the quasi-neutral regions that drops sharply to zero at the space-charge region edges (Fig. A-1(f)).

APPENDIX B

Determination of the Eigenvalues for SCCD and OCVD

In this report, we have two Eigenvalue equations, Eqs. (9) and (12), that determine s_i of each mode for OCVD and SCCD. These are

$$\coth(X_{QNB}(1 + s_i\tau_p)^{1/2}/L_p) + D_p(1 + s_i\tau_p)/L_pS_{eff} = 0 \qquad (9)$$

and

$$1 + (D_p(1 + s_i\tau_p)^{1/2}/L_pS_{eff})\coth(X_{QNB}(1 + s_i\tau_p)^{1/2}/L_p) = 0 \quad . \qquad (12)$$

In (9) and (12), Eigenvalues exist only if

$$1 + s_i\tau_p < 0 \text{ (or } s_i < -1/\tau_p \text{ or } \tau_i > \tau_p) \qquad (B\text{-}1)$$

where $\tau_i = -1/s_i$.

Granting (B-1), we have

$$(1 + s_i\tau_p)^{1/2} = j(-1-s_i\tau_p)^{1/2} \quad ,$$

where $(-1-s_i\tau_p) > 0$. Replacing $(1 + s_i\tau_p)^{1/2}$ in (9) and (11) with $j(-1-s_i\tau_p)^{1/2}$ yields

$$\cot(X_{QNB}K_i/L_p) - (D_pK_i/L_p) = 0 \qquad \text{(B-2)}$$

and

$$1 + (D_pK_i/L_pS_{eff})\cot(X_{QNB}K_i/L_p) = 0 \quad , \qquad \text{(B-3)}$$

where

$$K_i = (-1-s_i\tau_p)^{1/2} \quad .$$

Equations (9) and (B-2) are identical and so are (11) and (B-3) under the condition of (B-1). (B-2) and (B-3) imply an infinite number of Eigenvalues as shown in Figs. B-1 and B-2.

For SSCD the vanishing determinant of the inverse of matrix A of Eq. (6) provides an alternate method for determining the Eigenvalues s_i, but no such systematic method exists for OCVD. More details regarding this are planned for future publications.

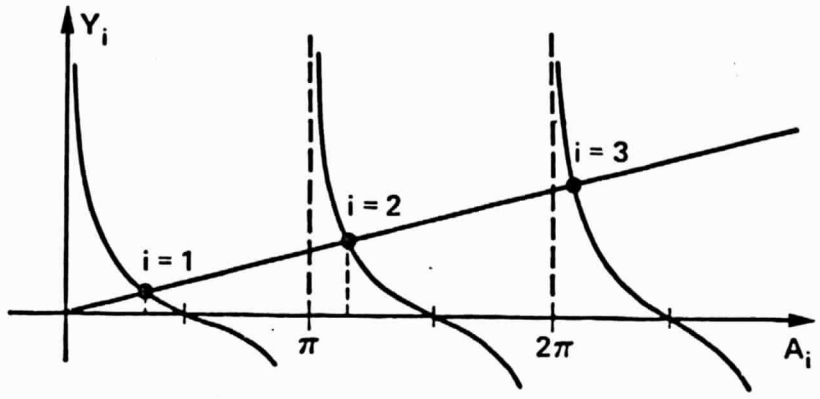

Fig. B-1 The eigenvalues for OCVD where $Y_i = \cot(A_i)$, $A_i = X_{QNB}K_i/L_P$ and $Y_i = (D_P S_{EFF}/X_{QNB})A_i$

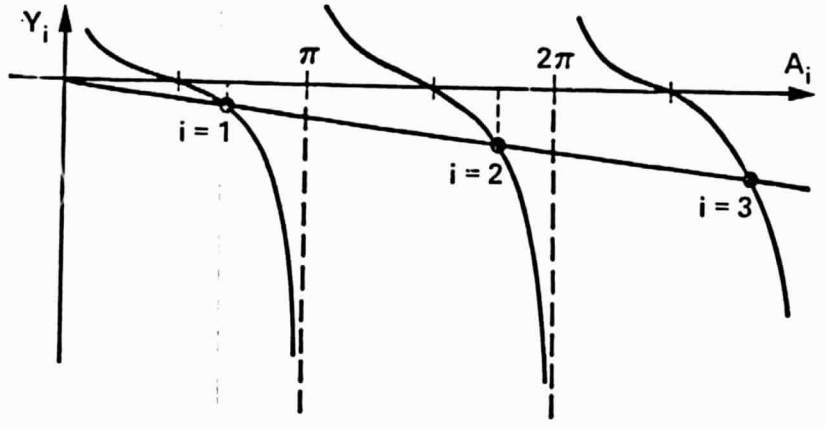

Fig. B-2 The eigenvalues for SCCD where $Y_i = \cot A_i$, $A_i = X_{QNB}K_i/L_P$ and $Y_i = -(X_{QNB}/D_P S_{EFF})A_i$

APPENDIX C

To obtain the base diffusion length L and effective surface recombination velocity S_{eff} at the back contact we have to solve the following two equations for the first-mode decay [2]:

$$1 + (D_p K_1 / L_p S_{eff}) \cot(W_{QNB} K_1 / L_p) = 0 \tag{C1}$$

$$i(0) = - \frac{qD_p P(0,0^-) K_1}{S_1 L_p} \frac{\cot(K_1 W_{QNB}/L_p) - (D_p K_1 / L_p S_{eff})}{(\tau_p / 2K_1^2) + (W_{QNB}/2S_{eff})[\mathrm{cosec}^2(K_1 W_{QNB}/L_p)]} \tag{C2}$$

Here $K_1 = (-1 - S_1 \tau_p)^{1/2}$, $S_1 = -1/\tau_{D1}$, W_{QNB} is the width of the quasi-neutral base, and $P(0, 0^-) = (n_i^2/N_{DD})[\exp(qV/kT) - 1]$ where V is the steady forward voltage applied for $t < 0$.

APPENDIX D

The small-signal quasi-neutral base capacitance and conductance are given by [4]:

$$C_{QNB}^{LF} = \frac{KD_n}{2L_n} \left[\frac{\frac{W_p D_n}{L_n} - \frac{L_n W_p^2 S_{eff}}{D_n} - S_{eff} L_n}{(\sinh^2 \frac{W_p}{L_n})(\frac{D_n}{L_n} \coth \frac{W_p}{L_n} + S_{eff})^2} + \right.$$

$$+ \tau_n \frac{\frac{D_n}{L_n} + S_{eff}\coth\frac{W_p}{L_n}}{\frac{D_n}{L_n}\coth\frac{W_p}{L_n} + S_{eff}}] \qquad \text{(D1)}$$

$$G_{QNB}^{LF} = \frac{KD_n}{L_n} \frac{\frac{D_n}{L_n} + S_{eff}\coth\frac{W_p}{L_n}}{\frac{D_n}{L_n}\coth\frac{W_p}{L_n} + S_{eff}} \qquad \text{(D2)}$$

where $K = Aq(q/kT)(n_i^2/N_{AA})\exp[(qV/kT) - 1]$.

REFERENCES

1. F. A. Lindholm and D. J. Hamilton, "A systematic modeling theory for solid-state devices", Solid-State Electron., vol. 7, pp. 771-783, 1964.

2. S. R. Lederhandler and J. J. Giacoletto, "Measurements of minority carrier lifetime and surface effects in junction devices", Proc. IRE, vol. 43, pp. 447-483, Apr. 1955.

3. R. H. Kingston, "Switching time in junction diodes and transistors," Proc. IRE, vol. 42, pp. 829-834, May 1954.

4. A. Neugroschel, P.J. Chen, S. C. Pao, and F. A. Lindholm, "Diffusion length and lifetime determination in p-n junction solar cells and diodes by forward biased capacitance measurements," IEEE Trans. Electron Devices, vol. ED-25, pp. 485-490, April 1978.

5. A. Neugroschel, "Determination of lifetime and recombination currents in p-n junction solar cells, diodes, and transistors," IEEE Trans. Electron Devices, vol. ED-28, pp. 108-115, Jan. 1981.

6. J. E. Mahan and D. L. Barns, "Depletion layer effects in the open circuit voltage decay lifetime measurements," Solid-State Electronics, vol. 24, pp. 989-994, 1981.

7. T. W. Jung, F. A. Lindholm, and A. Neugroschel, IEEE Trans. Electron Device, ED-31, 588, May 1984.

8. C. T. Sah, Physica Status Solidi(a), 7, 541, 1971.

9. A. Neugroschel, P. J. Chen, S. C. Pao, and F. A. Lindholm, IEEE Trans. Electron Devices, ED-25, 485(1978).

10. A. Neugroschel, IEEE Trans. Electron Devices, ED-28, 108(1981).

11. F. N. Gonzalez, A. Neugroschel, IEEE Trans. Electron Devices, ED-31, 413(1984).

12. M. A. Shibib, F. A. Lindholm, and F. Therez, IEEE Trans. Electron Devices, ED-26, 959(1979).

13. A. Neugroschel, F. A. Lindholm, and C. T. Sah, IEEE Trans. Electron Devices, ED-24, 662(1977).

14. H. C. de Graaff and J. G. de Groot, IEEE Trans. Electron Devices, ED-26, pp. 1771, 1979.

15. T. H. Ning and R. D. Isaac, IEEE Trans. Electron Devices, ED-27, pp. 2051, 1980.

16. A. A. Eltouckhy and D. G. Roulston, IEEE Trans. Electron Devices, ED-29, pp. 1862, 1984.

17. J. Godfrey and M. A. Green, IEEE Electron Device Letters, 1983

18. A. Neugroschel, F. A. Lindholm, and S. C. Pao, IEEE Trans. Electron Devices, 29, pp. 894, 1982.

19. P. T. Landsberg, A. Neugroschel, F. A. Lindholm, and C. T. Sah, Proc. 18th Photovoltaic Specialists Conf., Orlando, FL, IEEE, New York, 1984.

20. R. W. Keyes, Solid-State Communications, vol. 32, pp. 179, 1979.

21. R. W. Keyes, Comments Solid State Phys., 10, pp. 23, 1981.

22. M. A. Shibib and F. A. Lindholm, IEEE Trans. Electron Devices, 27, pp. 1304, 1980.